A role for nuclear envelope–bridging complexes in homology-directed repair

Rebecca K. Swartz, Elisa C. Rodriguez, and Megan C. King
Department of Cell Biology, Yale School of Medicine, New Haven, CT 06520

ABSTRACT **Unless efficiently and faithfully repaired, DNA double-strand breaks (DSBs) cause genome instability. We implicate a *Schizosaccharomyces pombe* nuclear envelope–spanning linker of nucleoskeleton and cytoskeleton (LINC) complex, composed of the Sad1/Unc84 protein Sad1 and Klarsicht/Anc1/SYNE1 homology protein Kms1, in the repair of DSBs. An induced DSB associates with Sad1 and Kms1 in S/G2 phases of the cell cycle, connecting the DSB to cytoplasmic microtubules. DSB resection to generate single-stranded DNA and the ATR kinase drive the formation of Sad1 foci in response to DNA damage. Depolymerization of microtubules or loss of Kms1 leads to an increase in the number and size of DSB-induced Sad1 foci. Further, Kms1 and the cytoplasmic microtubule regulator Mto1 promote the repair of an induced DSB by gene conversion, a type of homology-directed repair. *kms1* genetically interacts with a number of genes involved in homology-directed repair; these same gene products appear to attenuate the formation or promote resolution of DSB-induced Sad1 foci. We suggest that the connection of DSBs with the cytoskeleton through the LINC complex may serve as an input to repair mechanism choice and efficiency.**

Monitoring Editor
Karsten Weis
ETH Zurich

Received: Oct 2, 2013
Revised: Apr 28, 2014
Accepted: Jun 11, 2014

INTRODUCTION

DNA double-strand breaks (DSBs) threaten genome integrity in proliferating cells. Failure to faithfully repair DSBs can lead to microdeletions, mutation, gross chromosomal rearrangements, and cellular transformation. The mechanism that a cell uses to repair a DSB is largely determined by cell cycle stage: nonhomologous end joining (NHEJ) in G1 and homology-directed repair (HDR) in S and G2, when the sister chromatid is readily available for use as a template for repair (Symington and Gautier, 2011). Should repair using the sister chromatid as a donor fail, homologous sequences either on the sister chromosome or at an ectopic locus may be used as a donor template; however, use of such templates can lead to loss of heterozygosity or mutation (Malkova and Haber, 2012). The mechanisms by which DSBs encounter potential donor sequences and evaluate sequence homology have yet to be fully elucidated.

The linker of nucleoskeleton and cytoskeleton (LINC) complex spans the nuclear envelope (NE), allowing forces generated by the cytoplasmic cytoskeleton to be exerted on chromatin inside the nucleus (Chikashige *et al.*, 2007; King *et al.*, 2008; McGee *et al.*, 2009). LINC complexes are composed of Sad1/Unc84 (SUN) and Klarsicht, Anc1, SYNE1 homology (KASH) domain proteins (Tapley and Starr, 2012). SUN proteins span the inner nuclear membrane and are characterized by the C-terminal SUN domain that protrudes into the lumen of the NE (Razafsky and Hodzic, 2009). The SUN domain mediates interactions with the tail-anchored KASH proteins, which span the outer nuclear membrane (Sosa *et al.*, 2012). Whereas the nuclear domains of SUN proteins interact with chromatin and the nuclear lamina, the cytoplasmic domains of KASH proteins interact with cytoskeletal filaments and/or motor proteins (Tapley and Starr, 2012). During meiosis, the LINC complex drives the formation of the meiotic bouquet and is essential for homologous chromosome pairing after programmed DSB formation (Scherthan *et al.*, 1996; Bass *et al.*, 2000; Niwa *et al.*, 2000; Vazquez *et al.*, 2002; Sato *et al.*, 2009; Yoshida *et al.*, 2013).

Recently the *Saccharomyces cerevisiae* SUN protein Mps3 was shown to be required for the localization of persistent DSBs to the nuclear periphery during S/G2 (Kalocsay *et al.*, 2009; Oza *et al.*, 2009), and increased levels of DNA damage have been observed in *Sun1*$^{-/-}$*Sun2*$^{-/-}$ mice (Lei *et al.*, 2012). Although both the SUN

This article was published online ahead of print in MBoC in Press (http://www.molbiolcell.org/cgi/doi/10.1091/mbc.E13-10-0569) on June 18, 2014.

Address correspondence to: Megan C King (megan.king@yale.edu).

Abbreviations used: DDR, DNA damage response; DSB, DNA double-strand break; GC, gene conversion; HDR, homology-directed repair; HU, hydroxyurea; iMTOC, interphase microtubule-organizing center; KASH, Klarsicht, Anc1, SYNE1 homology; LINC, linker of nucleoskeleton and cytoskeleton; MBC, carbendazim; MCL, minichromosome loss; MMS, methyl methanesulfonate; MT, microtubule; NE, nuclear envelope; NHEJ, nonhomologous end joining; SCC, sister chromatid conversion; SPB, spindle pole body; SUN, Sad1/Unc84.

proteins and the tethering of DSBs to the nuclear periphery have been implicated in regulating DSB repair, the role of KASH proteins and their connection to the cytoskeleton has not been investigated. The *Schizosaccharomyces pombe* genome encodes two canonical KASH proteins, Kms1 and Kms2, along with one SUN protein, Sad1. Sad1 and Kms2 are reported to be essential, likely due to their roles at the spindle pole body (SPB) during mitotic division (Hagan and Yanagida, 1995; Ding *et al.*, 2000; Kim *et al.*, 2010; Wälde and King, 2014). Although Kms1 is important for successful meiosis (Shimanuki *et al.*, 1997; Yoshida *et al.*, 2013), it is not essential for viability, and thus far a function for Kms1 during vegetative growth has not been described. Here we implicate the NE-spanning *S. pombe* Sad1-Kms1 LINC complex and its connection to microtubules (MTs) in facilitating HDR of resected DSBs.

RESULTS

Induced, site-specific DSBs associate with Sad1

In *S. cerevisiae*, persistent DSBs associate with the nuclear periphery in a SUN protein–dependent manner; however, the studies reporting this did not directly assess this association by microscopy (Kalocsay *et al.*, 2009; Oza *et al.*, 2009). To examine whether DSBs associate with Sad1 in *S. pombe*, we first incorporated an HO-endonuclease recognition site (Rudin and Haber, 1988) at either the *ade8* or *ade3* locus in cells expressing mCherry fused to Rad52 (also named Rad22). Twenty-four hours after derepression of HO-endonuclease driven from the *nmt41* (*no message in thiamine*) promoter (Osman *et al.*, 1996; Prudden *et al.*, 2003), we observed a single focus of Rad52-mCherry in 60–70% of cells compared with ~2% of uninduced cells, establishing robust induction of the site-specific DSB (Supplemental Figure S1A). This long time course of induction is required due to the relatively slow and asynchronous induction of *nmt41* after removal of thiamine from the culture (Basi *et al.*, 1993), making it likely that many of the DSBs observed here are persistent. In live cells, we observed a subset of induced DSBs closely associated with Sad1–green fluorescent protein (GFP) at the SPB (Figure 1A, asterisks). In *S. pombe*, the SPB constantly oscillates along the NE in a MT-dependent manner. Monitoring the position of the DSB and Sad1 over time, we find that these signals remain associated as the SPB oscillates for >30 min (Figure 1A and Supplemental Video S1). Quantitating a greater number of cells (taken from at least three replicate experiments, each containing >50 cells with induced DSBs), we find that ~25% (at *ade3*) to ~40% (at *ade8*) of the induced DSBs comigrate with Sad1-GFP over the entire experimental time course of at least 10 min (Figure 1B).

In budding yeast, induced DSBs associate with the NE in asynchronously growing (but not in G1-arrested) cultures (Oza *et al.*, 2009). In asynchronous populations of *S. pombe*, the vast majority of cells are in the G2 phase of the cell cycle. Thus we arrested cells in G1 to assess whether cell cycle stage affected association of DSBs with Sad1. DSBs induced in G1 may not efficiently recruit Rad52 because HDR is repressed (Symington and Gautier, 2011; Ferretti *et al.*, 2013; Tomimatsu *et al.*, 2014). Therefore we tested the cell cycle dependence of DSB-Sad1 association using a system in which a lac operator array is integrated near the HO-endonuclease site at *ade8* in cells expressing lacI-GFP and Sad1-mCherry (Straight *et al.*, 1996; Ding *et al.*, 2004). In cells that were arrested in G1 through nitrogen deprivation with concomitant induction of the DSB, we did not observe an association between the lac operator array and Sad1-mCherry (Figure 1, C and D). Thus we conclude that persistent DSBs arising in S/G2 can be recruited to Sad1, leading to their association with the oscillating SPB.

Sad1 complexes assemble in response to DNA damage

Owing to the slow and asynchronous induction of the *nmt41* promoter, we used an alternate assay to investigate the acute effect of DSBs on Sad1 appearance. To that end, we monitored Sad1-mCherry in cells treated with methyl methanesulfonate (MMS), a DNA-alkylating agent that leads to replication fork collapse and, ultimately, DSBs (Beranek, 1990). After adding MMS, we observed a progressive increase in the number of Sad1 foci within the NE over time (Figure 2, A, arrows, and B), suggesting localized accumulation of Sad1, possibly in higher-order complexes, at non-SPB sites in response to DSBs. This change in Sad1 appearance did not correspond to an increase in expression of Sad1 (Supplemental Figure S1B). Because the copy number of Sad1 in the SPB is established (450–1030 polypeptides at the SPB; Wu and Pollard, 2005), we can use ratiometric experiments to estimate that these MMS-induced Sad1 foci contain 200–500 copies of Sad1-mCherry (see *Materials and Methods* and Supplemental Figure S1C). Further, we can estimate that our measurements can only reliably identify a Sad1 focus that contains >100–250 copies of Sad1-mCherry.

We next examined whether ATR and/or ATM, the master regulatory kinases of the DNA damage response (DDR), are necessary for the ability of Sad1 to respond to DNA damage. In *S. pombe*, the ATR homologue Rad3 plays a more prominent role than the ATM homologue Tel1 in the DDR, particularly in G2 (Labib and De Piccoli, 2011). In cells lacking Rad3, the number of Sad1-mCherry foci that arose after MMS treatment was strongly attenuated (Figure 2C), suggesting that ATR is required to stimulate Sad1 foci formation in response to DNA damage. By contrast, loss of Tel1 does not prevent formation of Sad1-mCherry foci in response to MMS (Supplemental Figure S1D). It has been suggested that the DDR undergoes a "switch" from acting through ATM to acting through ATR that coincides with the production of extended single-stranded DNA overhangs due to resection (Shiotani and Zou, 2009); indeed, extensive resection is one of the processes that distinguishes HDR from other DSB repair pathways. In *S. pombe*, efficient long-range resection depends on the exonuclease Exo1 (Langerak *et al.*, 2011). Therefore we examined the response of Sad1 after MMS treatment in *exo1Δ* cells. After 3 h in MMS, <12% of *exo1Δ* cells had multiple Sad1-mCherry foci, significantly less than wild-type (WT) cells (Figure 2C). Thus we conclude that the ATR kinase and long-range resection are required for Sad1 foci to form in response to DNA damage.

Sad1 colocalizes with Kms1 along MTs

We were curious about whether the MMS-induced Sad1 foci also associated with the KASH proteins Kms1 and/or Kms2. Although Kms1 has been characterized for its roles in meiosis (Shimanuki *et al.*, 1997; Yoshida *et al.*, 2013), we verified that the *kms1* transcript and hemagglutinin (HA)-Kms1 under the control of its endogenous promoter are expressed in vegetatively growing cells (Supplemental Figure S2, A–D), consistent with recent genome-wide data sets (Marguerat *et al.*, 2012). We found that the number of Kms1 (but not Kms2) foci increased in response to MMS treatment (Figure 2, A and B, and Supplemental Figure S1, E and F), although this was not significant until 3 h after MMS addition. Because a small proportion of untreated cells contain multiple Sad1 and Kms1 foci (Figure 2B), we wondered whether Sad1-Kms1 foci outside the SPB might be a form of noncentrosomal interphase microtubule-organizing center (iMTOC; Sawin and Tran, 2006). Consistent with this notion, we find Sad1 and Kms1 colocalized in detectable foci outside the SPB in a small proportion of untreated cells (4%; Supplemental Figure S3A), and Sad1-mCherry colocalizes with

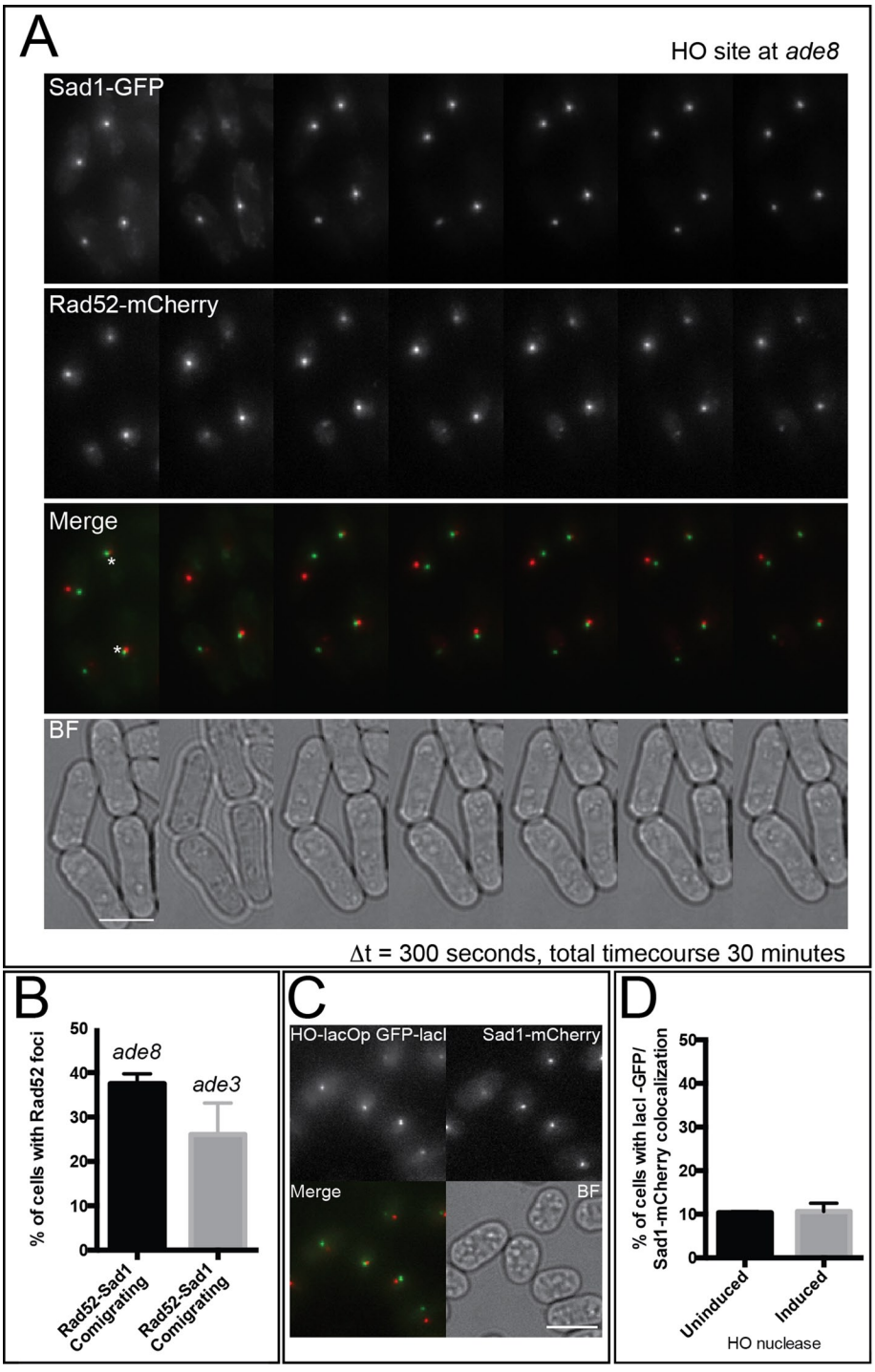

FIGURE 1: Site-specific DSBs comigrate with Sad1 at the spindle pole body in S/G2. (A) Maximum-intensity projection time course (eight *Z*-sections with 0.5-µm spacing, EM-CCD camera) of MKSP1185 cells expressing Sad1-GFP and Rad52-mCherry after induction of a site-specific HO DSB at *ade8*. Asterisks indicate cells in which the Sad1 and the DSB associate and comigrate over the 30-min time course. (B) Percentage of cells with a Rad52-mCherry focus in which Rad52 associates with Sad1-GFP (MKSP1185 *ade3*, and MKSP1674, *ade8*) for the entire time course (>10 min). Values are the mean ± SD of at least three experiments each evaluating at least 100 cells. (C) Representative maximum-intensity projection (eight *Z*-sections with 0.5-µm spacing, EM-CCD camera) of induced, G1-arrested MKSP1498 cells containing a lac operator array near an HO recognition site and expressing Sad1-mCherry and lacI-GFP. (D) Percentage of cells in which Sad1 associates with the GFP-lacI focus with and without induction of the HO nuclease. Values are the mean ± SD of at least three experiments each evaluating at least 100 cells. BF, brightfield image. Scale bars, 5 µm.

the γ-tubulin subunit Alp4-GFP (Horio *et al.*, 1991) at both the SPB and these noncentrosomal iMTOCs (Supplemental Figure S3B). Further, both Sad1 and Kms1 at iMTOCs are found in association with MTs (Supplemental Figure S3, C and D). We also found that, as for Sad1-GFP (Figure 1, A and B), ~40% of site-specific induced DSBs at *ade8* comigrate with GFP-Kms1 at the SPB (Figure 3, A and B, and Supplemental Video S2). In addition, we found that about three-fourths of Sad1-mCherry foci induced by MMS treatment can be found along MTs (Figure 3, C and D). Moreover, tracking of DSBs associated with the SPB are significantly more mobile over the minutes time scale than those that remain unassociated (Figure 3E). Taken together, these results raise the possibility that Sad1 and Kms1 in the form of iMTOCs coalesce in response to DNA damage. Further, if left unrepaired, DSBs become associated with the SPB, which leads to an increase in DSB mobility.

Impaired HDR increases DDR-induced Sad1-Kms1 LINC complex number

The observation that ATR and resection are necessary for the Sad1 DDR suggests that Sad1-Kms1 LINC complex foci may be related to HDR. To better place the MMS-induced formation of Sad1-Kms1 foci in this context, we examined the effect of depleting Rad51, a key protein that promotes strand invasion during HDR (Sauvageau *et al.*, 2005). Consistent with previous work showing that *rad51Δ* cells display increased genome instability (Muris *et al.*, 1997), we observed a significantly greater number of Sad1-Kms1 foci in untreated *rad51Δ* cells compared with WT cells: ~30% of untreated *rad51Δ* cells had multiple Sad1-mCherry foci, and >7% of *rad51Δ* cells had multiple GFP-Kms1 foci, compared with 13 and 4% of WT cells, respectively (Figure 3F). On treatment with MMS, the number of Sad1-Kms1 foci was also greater in *rad51Δ* cells than in WT cells (Figure 3F). Thus, unlike resection, strand invasion is dispensable for MMS to induce formation of Sad1-Kms1 foci. Further, Rad51-dependent repair appears to attenuate the formation or lifetime of DSB-induced Sad1-Kms1 foci.

Loss of Kms1, Mto1, or MT depolymerization alters the DDR of Sad1

We next investigated the effect of depleting Kms1 on the association of the site-specific induced DSB with Sad1. We did not detect a loss of DSBs associated with Sad1 at the SPB in *kms1Δ* compared with

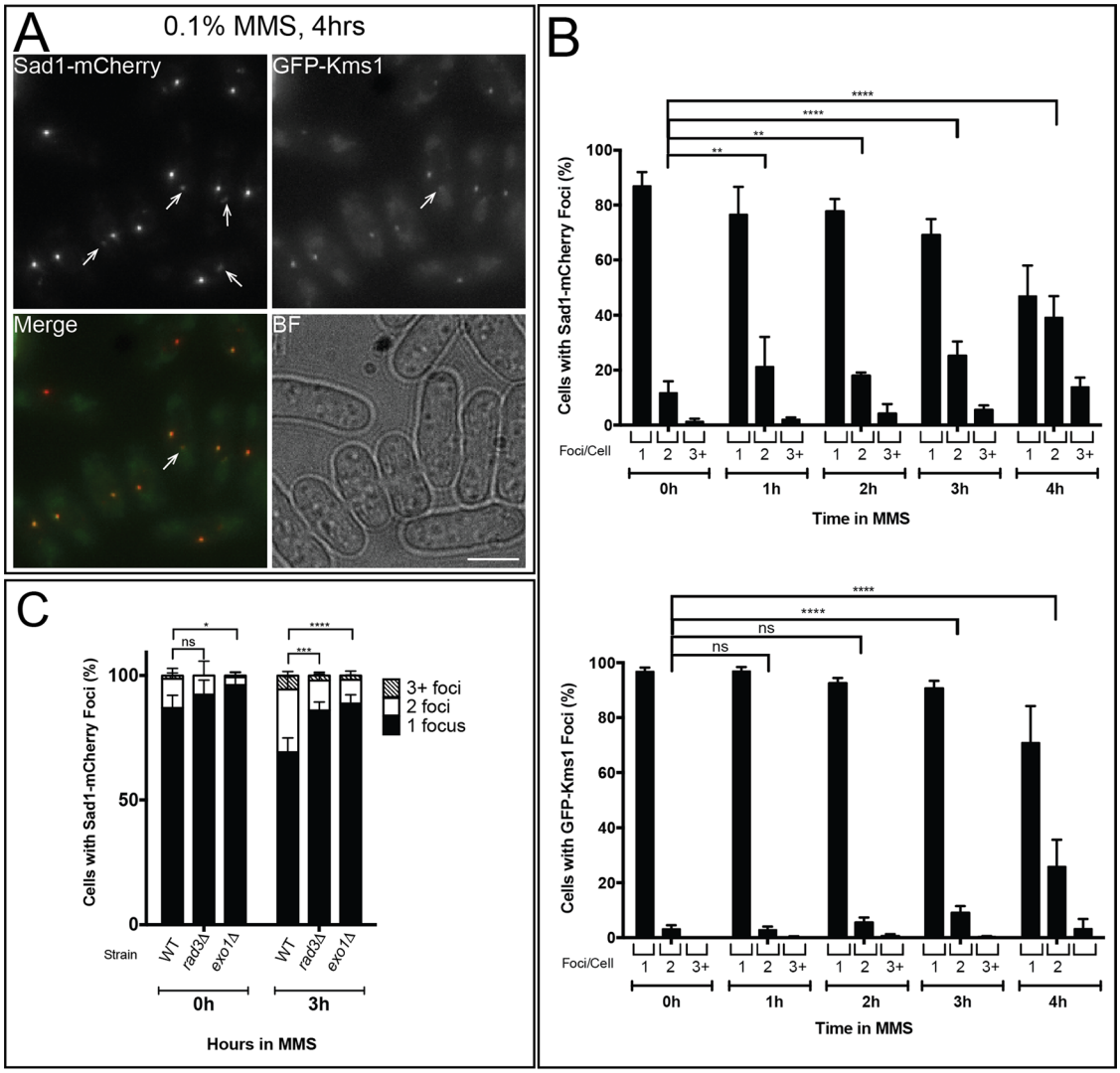

FIGURE 2: MMS induces foci of Sad1 within the NE in an ATR- and resection-dependent manner. (A) Representative maximum-intensity projection (14 *Z*-sections with 0.3-µm spacing, CCD camera) of MKSP754 cells expressing Sad1-mCherry and GFP-Kms1 after 4 h of exposure to 0.1% MMS. Arrows indicate noncentrosomal foci of Sad1 and/or Kms1. (B) Quantification of the number of Sad1-mCherry and GFP-Kms1 foci before and after 1–4 h of exposure to 0.1% MMS. Values are averages with SD of at least three experiments each evaluating at least 100 cells. Statistical significance was determined by pooling the three experiments and treating the population as a multinomial distribution, followed by a Chi-squared test to determine *p* values. (C) Quantification of the number of Sad1-mCherry foci in WT, *rad3Δ* (MKSP1290), or *exo1Δ* (MKSP1233) cells before and after 3 h of exposure to 0.1% MMS. Foci were counted as described in B. *$p < 0.05$,**$p < 0.01$, ***$p < 0.001$, ****$p < 0.0001$. Scale bars, 5 µm.

WT cells (Figure 4A). However, in ~15% of cells lacking Kms1 (but very rarely in WT cells), we observed the induced DSB in association with Sad1 outside the SPB (Figure 4A, arrows). To further investigate how nuclear inputs (DNA damage) and cytoskeletal inputs (MTs) might together affect the response of Sad1 to DNA damage, we monitored Sad1-mCherry in MMS-treated cells in the absence of Kms1 or Mto1. Mto1 (also known as Mod20 or Mbo1) contributes to normal MT dynamics in interphase but is dispensable during mitosis (Sawin *et al.*, 2004; Venkatram *et al.*, 2004). Of interest, we observed more-rapid accumulation of Sad1-mCherry foci in MMS-treated cells in the absence of Kms1 or Mto1 than with WT cells, with a more pronounced effect in *kms1Δ* cells (Figure 4, B and C). Further, the MMS-induced Sad1-mCherry foci were significantly more intense in *kms1Δ* cells compared with WT (Supplemental Figure S4A).

Given that Kms1 provides the physical link between Sad1 and MTs and Mto1 is required for normal MT dynamics, we predicted that depolymerizing MTs would phenocopy the loss of Kms1 or Mto1 during the DDR. Indeed, in cells expressing Sad1-mCherry and GFP-Kms1 that are treated with both MMS and carbendazim (MBC), a MT-depolymerizing drug, Sad1- and Kms1-containing foci appeared in greater number after 1 h than in cells treated with MMS alone (Figure 4, D and E). This is likely an underestimate of this effect, as a short time course is necessary to avoid mitotic arrest due to spindle disruption (mitotically arrested cells were excluded from the analysis). As in *kms1Δ* cells, these Sad1-mCherry foci were significantly more intense when cells were treated concomitantly with MMS and MBC than with MMS alone (Supplemental Figure S4B). Further, in both *kms1Δ* cells treated with MMS and WT cells treated with MBC plus MMS, we see the accumulation of large "platforms"

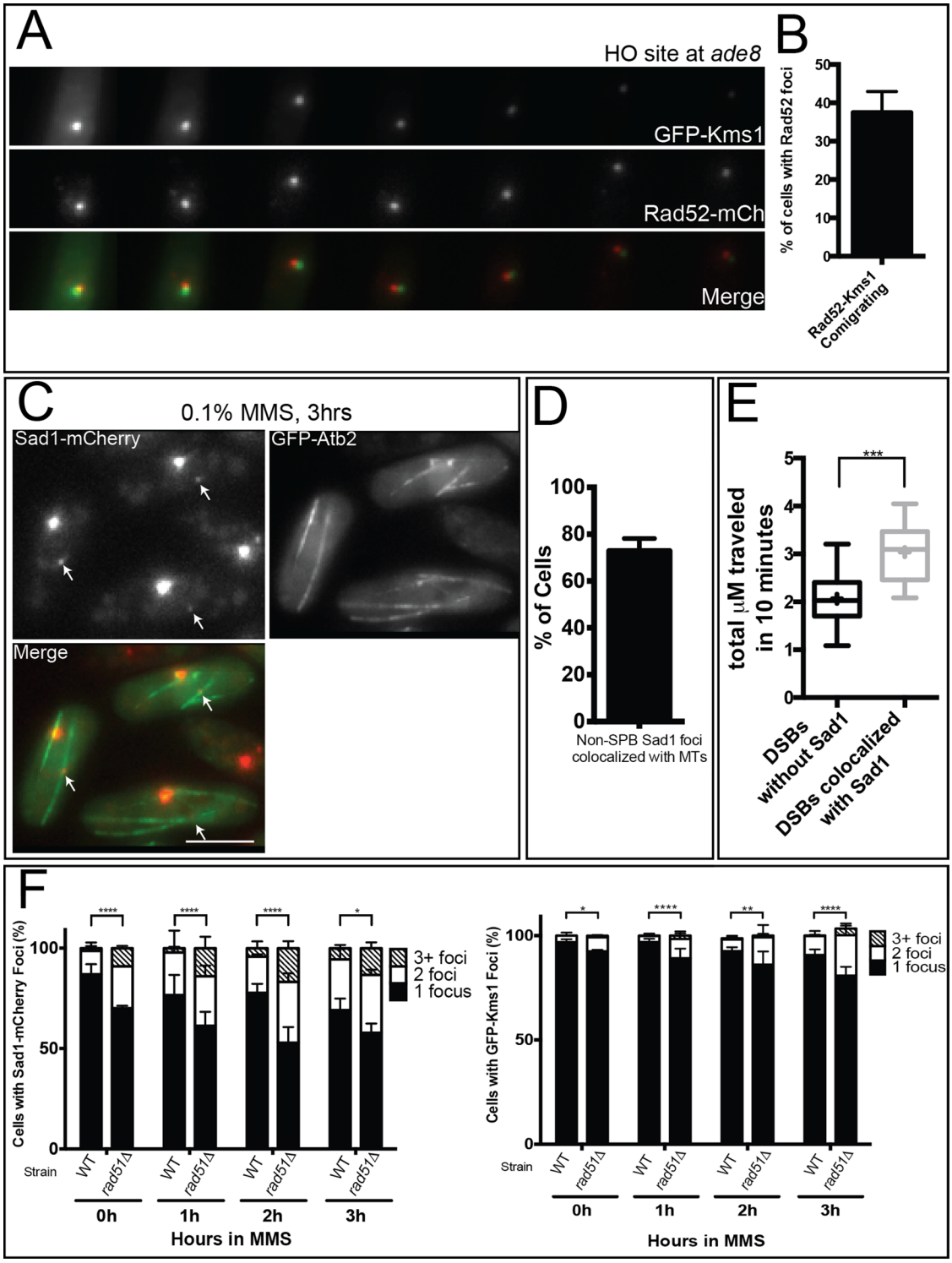

FIGURE 3: DSBs comigrate with Kms1 along MTs. (A) Maximum-intensity projection time course (eight *Z*-sections with 0.5-μm spacing, EM-CCD camera) of a MKSP411 cell expressing GFP-Kms1 and Rad52-mCherry after induction of the HO DSB at *ade8*. (B) Quantification of the percentage of interphase cells with a Rad52-mCherry focus in which Rad52 associates with GFP-Kms1 (MKSP411) for the entire time course. Values are the mean ± SD of at least three experiments each evaluating at least 100 cells. (C) Maximum-intensity projections (10 *Z*-sections with 0.4-μm spacing, EM-CCD camera) of MKSP1079 cells expressing Sad1-mCherry and GFP-Atb2 exposed to 0.1% MMS for 3 h. (D) Quantification of the number of MMS-induced Sad1 foci found along MTs ($n = 31$ cells). (E) Plot of the distance traveled by an induced DSB at *ade3* over 10 min (visualized by Rad52-mCherry) grouped according to their association with Sad1-GFP. Maximum-intensity projections were generated from raw time-lapse movies, followed by particle tracking using the Manual Tracking plug-in in Image J. $n > 20$ cells each. (F) Quantification of Sad1-mCherry and GFP-Kms1 foci in *rad51Δ* cells (MKSP1204) either untreated or after 0.1% MMS treatment for 1–3 h. Foci were counted as described in Figure 2B. BF, brightfield image *$p < 0.05$, **$p < 0.01$, ***$p < 0.001$, ****$p < 0.0001$. Scale bars, 5 μm.

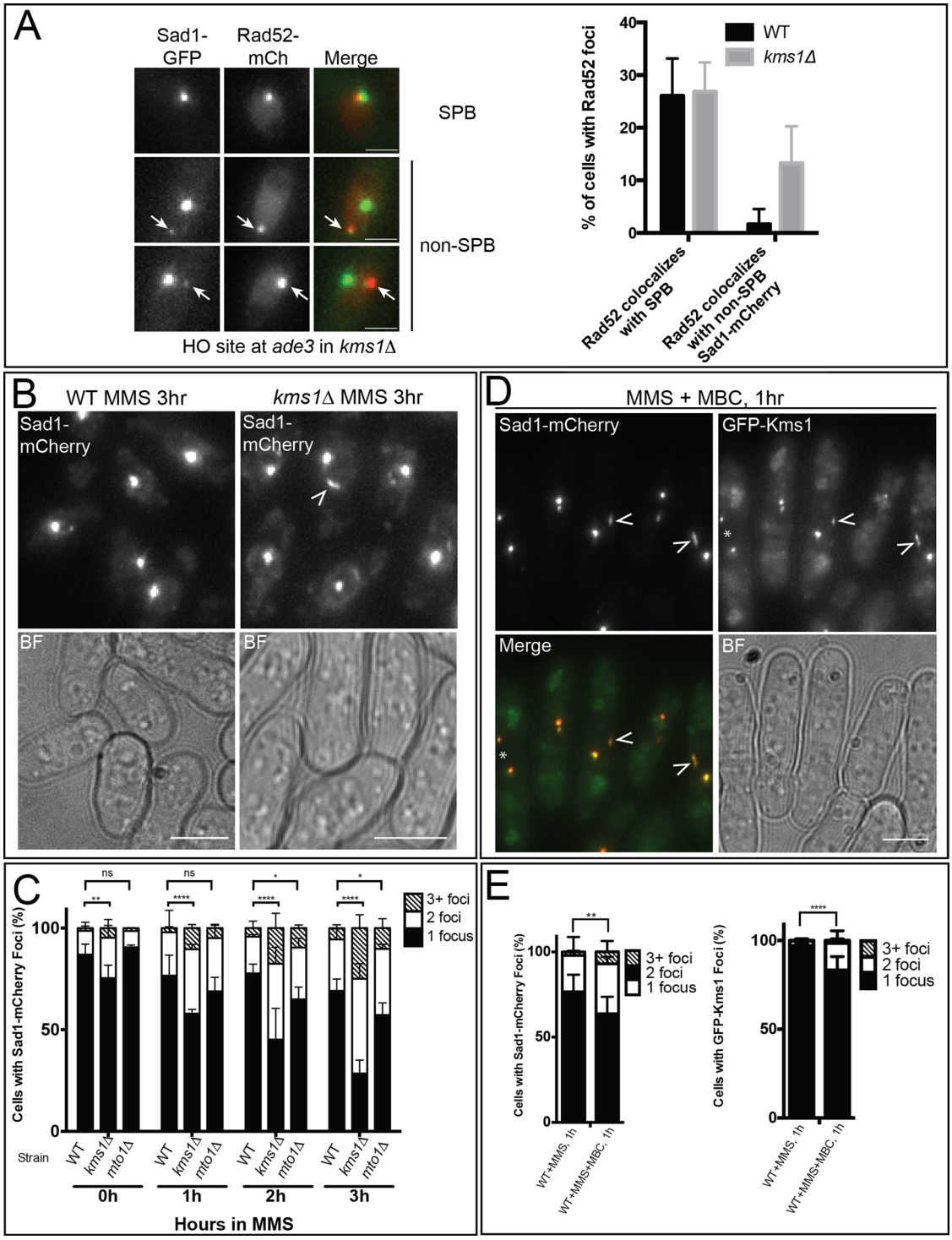

FIGURE 4: Loss of Kms1, Mto1, or MTs alters the DDR response of Sad1. (A) A population of persistent DSBs associated with Sad1 reside outside the SPB region in the absence of Kms1. Maximum-intensity projections (12 *Z*-sections with 0.4-μm spacing, EM-CCD camera) of *kms1Δ* cells expressing Sad1-GFP and Rad52-mCherry after induction of a site-specific HO DSB at *ade3*. Representative examples of an SPB-associated DSB and two non–SPB-associated DSBs. Scale bars, 1 μm. The percentage of DSBs associated with Sad1 was analyzed and is plotted as in Figure 1B. (B) Maximum-intensity projections (14 *Z*-sections with 0.3-μm spacing, CCD camera) of Sad1-mCherry foci in *kms1Δ* cells (MKSP1086) exposed to 0.1% MMS for 3 h. (C) Quantification of Sad1-mCherry foci in WT, *kms1Δ* (MKSP1086), and *mto1Δ* (MKSP 1571) cells with and without 0.1% MMS exposure. *$p < 0.05$, **$p < 0.01$, ***$p < 0.001$, ****$p < 0.0001$. (D) Maximum-intensity projections (14 *Z*-sections with 0.3-μm spacing, CCD camera) of Sad1-mCherry foci and GFP-Kms1 foci in cells (MKSP754) treated with MMS plus MBC for 1 h. (E) Quantification of Sad1-mCherry and GFP-Kms1 foci in cells (MKSP754) treated with MMS plus MBC for 1 h. Arrowheads in B and D indicate large "platforms" of Sad1 (B) or Sad1 and Kms1 (D). Asterisk in D indicates an example of a mitotically arrested cell that was excluded from data analysis. Foci were counted as described in Figure 2B. BF, brightfield image. *$p < 0.05$, **$p < 0.01$, ***$p < 0.001$, ****$p < 0.0001$. Scale bars, 5 μm.

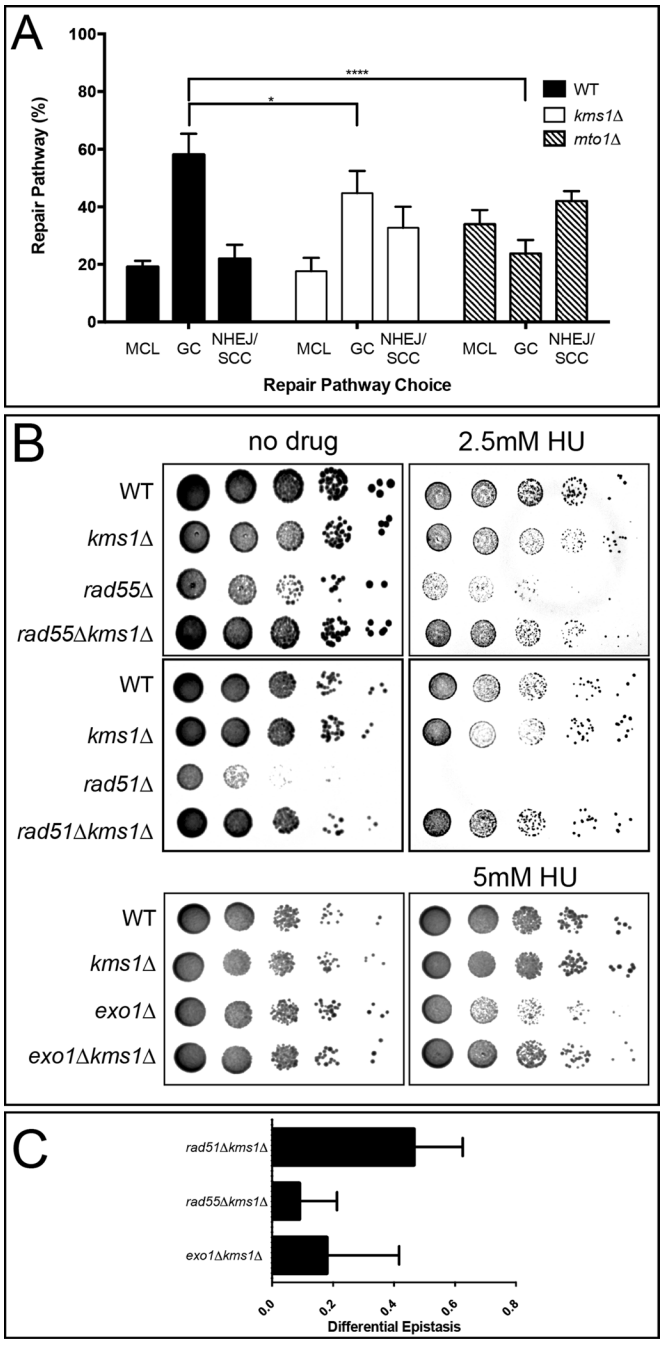

FIGURE 5: Kms1 and Mto1 promote HDR. (A) Repair pathway choice for an induced, site-specific DSB in WT, *kms1*Δ, and *mto1*Δ cells. GC, gene conversion; MCL, minichromosome loss; SCC/NHEJ, sister chromatid conversion/nonhomologous end joining. *$p < 0.05$, **$p < 0.01$, ***$p < 0.001$, ****$p < 0.0001$. (B) Suppressive genetic interactions between *kms1* and genes important for HDR, including the strand invasion proteins Rad55 and Rad51 and the exonuclease Exo1. Serial dilutions, 1:10, were grown on YE5S plates with or without HU as indicated to reveal growth defects specifically in response to DNA damage. (C) Differential epistasis analysis of the genetic interactions shown in B. Differential epistasis was calculated by subtracting the epistasis deviation of double-knockout cells on plates containing HU from YE5S plates. Epistasis deviation is the difference between the expected epistasis and actual epistasis of the double-knockout cells. Epistasis values were determined as a ratio of knockout average colony size to WT average colony size. Expected epistasis of double-knockout strains is the product of the epistasis values of both single-knockout strains.

of Sad1-mCherry that we do not observe in WT cells (Figure 4, B and D, arrowheads), likely a consequence of increased Sad1 copy number and/or relaxation of the defined focal nature of Sad1 in the absence of MT forces.

Kms1 promotes gene conversion

Because association of DSBs with Sad1 appears independent of Kms1 (Figure 4, A and B), the *kms1Δ* background provides an experimental system in which we can uncouple the mechanical connection between DSBs inside the nucleus from cytoplasmic MTs while leaving sequestration of DSBs at the NE unaffected. To explicitly test whether loss of Kms1 affects DSB repair, we used an established system in which an induced DSB is formed on a minichromosome derived from chromosome III (Prudden *et al.*, 2003), allowing for viability even when the DSB remains unrepaired. The readout for HDR in this assay relies on a pathway similar to interallele gene conversion (GC) in which the endogenous chromosome III is used as a template for repair of the chromosome III–derived minichromosome. Of importance, if repair occurs via sister chromatid conversion (SCC), in which the sister chromatid is the template for HDR, the inducible DSB site is restored and will have the same genetic markers as before DSB induction. We found that WT *S. pombe* use the GC pathway with an efficiency of 58% (Figure 5A). *kms1Δ* cells are significantly less efficient at using GC, with GC rates ~13% lower than WT (Figure 5A). Concomitant with the decreased GC rates in *kms1*Δ cells, the rate of NHEJ/SCC increased compared with WT cells. The rate of minichromosome loss (MCL; the readout for failed repair) did not increase (Figure 5A). If the contribution of Kms1 to HDR involves bridging the DSB to cytoplasmic MTs, we would expect that perturbations to MT dynamics would also influence DSB repair outcome. Indeed, in cells lacking Mto1, rates of GC fell significantly to <30%, whereas rates of MCL (failed repair) and NHEJ/SCC both increased (Figure 5A). This suggests that cytoplasmic MT dynamics can promote GC events, in part through Kms1.

kms1 genetically interacts with established HDR factors

To better understand the cellular consequences of disrupting the connection of Sad1-associated DSBs with MTs, we challenged *kms1Δ* cells with various types of DNA damage (MMS, hydroxyurea [HU] or camptothecin). On its own, loss of Kms1 does not appear to compromise growth or viability in the presence of these agents (Supplemental Figure S5A), consistent with a model in which Kms1 is not essential for DNA repair but instead affects DNA repair pathway choice. Because we observed that a greater number of Sad1-Kms1 foci occur in certain genetic backgrounds (such as *rad51Δ*), we carried out a limited genetic analysis between *kms1* and established DNA repair factors. We failed to observe genetic interactions between *kms1* and NHEJ factors such as Ku70, as well as other factors recruited early after DSB formation, such as components of the 9-1-1 complex (Hus1, Rad9; Supplemental Figure S5B). By contrast, we found that *kms1* genetically interacts with a variety of genes involved in HDR (Figure 5B). In particular, *kms1*Δ suppresses the growth phenotypes of *rad55*Δ, *rad51*Δ, and *exo1*Δ on plates containing HU while also suppressing the growth defect of *rad51*Δ cells on rich media that likely occurs due to spontaneous DNA damage (Muris *et al.*, 1997). The ability of DNA damage to potentiate these suppressive genetic interactions could be quantitatively assessed by measuring the differential epistasis with and without HU (Figure 5C). We do not see such a genetic interaction with a repressible allele of Kms2 (*kms2 DAmP*) that leads to Kms2 depletion (Wälde and King, 2014; Supplemental Figure S5C), consistent with the observation that Kms2 is not recruited to MMS-induced Sad1 foci (Supplemental

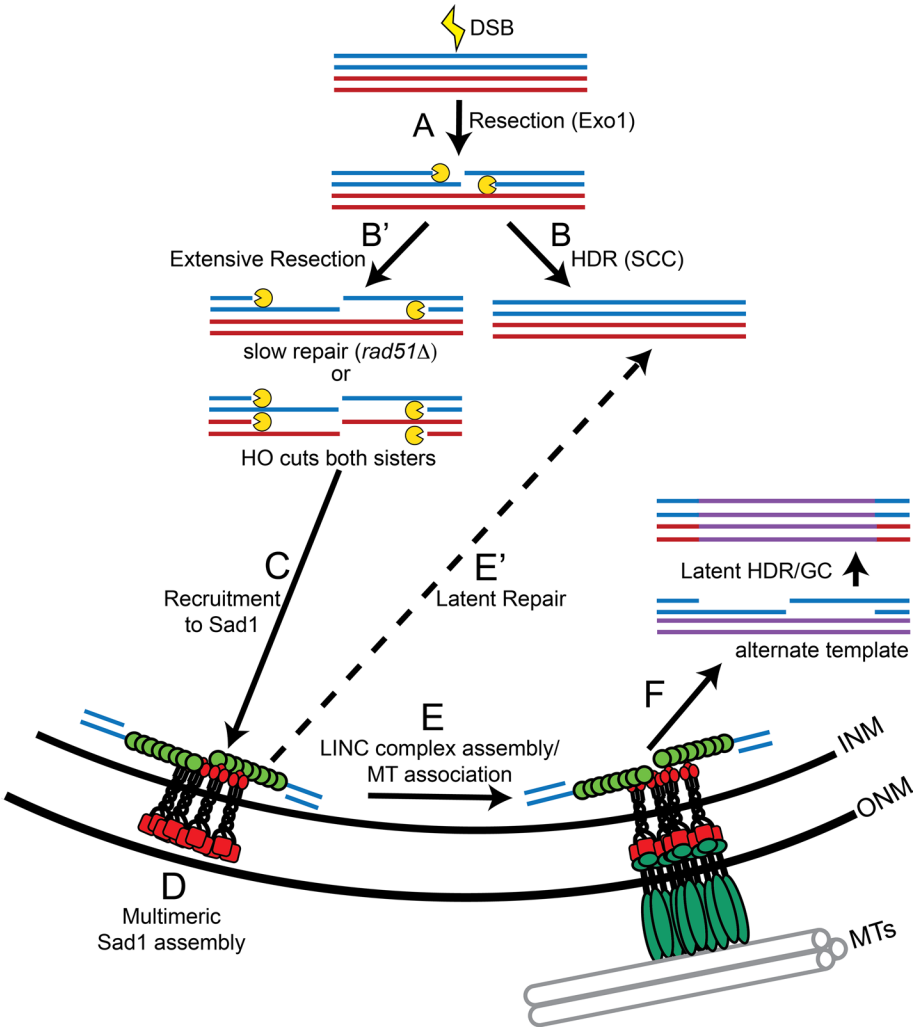

FIGURE 6: Model for the role of the LINC complex in HDR. In G2 cells, DSBs are resected (A) and can be repaired through sister-chromatid conversion (B). When SCC fails or is prevented by DSBs on both sisters, resection continues and becomes extensive (B'). Extensively resected DSBs are recruited to Sad1 (C), which stimulates Sad1 to coalesce into foci (D). Sad1 either constitutively or in response to its multimeric assembly recruits Kms1, forming a complete LINC complex that can associate with MTs (E). Coupling of the DSB to MTs through the Sad1-Kms1 LINC complex can then promote repair of the DSB by GC using alternate templates (F), which may involve or lead to association with the SPB. When a Sad1-associated DSB is not connected to MTs through Kms1, latent repair can still occur through alternative pathways (E').

Figure S1F). Further, *mto1*Δ cells, which show a more profound defect in the DNA repair assay, are sensitive to a variety of DNA-damaging agents (Supplemental Figure S5D). These genetic data support a model in which cytoplasmic MTs, and their connection to DSBs within the nucleus, can affect HDR.

DISCUSSION

Here we provide evidence that the nuclear membrane–spanning Sad1-Kms1 LINC complex contributes to DSB repair, specifically HDR. We show for the first time that DSBs promote the formation of (and associate with) LINC complexes, which can mechanically link DSBs to the MT cytoskeleton. The ATR kinase and resection are required for Sad1-Kms1 foci formation in response to DSBs, whereas loss of Rad51 or Mto1 or depolymerization of MTs leads to an increase in the number and size of Sad1 foci in response to MMS. Most important, Kms1 and Mto1 promote repair of DSBs through GC, and loss of Kms1 can suppress the growth phenotypes of HDR mutants such as *rad51*Δ.

A model for LINC complex function in the DDR

In *S. pombe* cells that have undergone DNA replication, we imagine that most repair proceeds with limited resection of the DSB (Figure 6A). If the DSB is efficiently repaired through the canonical HDR pathway using the nearby sister chromatid as a template (Figure 6B), resection is restrained, ATR activation is minimal, and the LINC complex does not contribute to repair. However, when repair is inefficient, either because of compromised HDR or because both sister chromatids are broken, as often occurs with induction of DSBs using HO-endonuclease (Figure 6B'), resection continues, ATR is activated, and the DSB is recruited to the NE, where it associates with Sad1 (Figure 6, C and D). Of interest, loss of the *S. cerevisiae* ATR homologue Mec1 also compromises recruitment of an irreparable DSB to the NE, although this was observed in the context of recruitment of DSBs to the SUMO-dependent ubiquitin ligase Slx5/Slx8 at the nuclear pore complex (Nagai *et al.*, 2008). Nevertheless, the SUN protein Mps3 may also play a role in recruitment of DSBs upstream of their interaction with Slx5/Slx8 (Gartenberg, 2009; Oza *et al.*, 2009). Understanding the temporal association of DSBs with different complexes at the NE remains a key challenge for further studies; *S. pombe* may prove a fruitful model system with which to address these questions, as we can directly visualize association of DSBs with Sad1 and Kms1. Either association of the DSB with preexisting Sad1-Kms1 complexes or sequential Sad1 and Kms1 binding (Figure 6D) leads to association with MTs (Figure 6E). The coupling of the DSB to MTs through the LINC complex may promote access to alternative HDR templates, including the homologous chromosome or other nonallelic sequences (Figure 6F). Should the DSB persist, this MT mobility may also lead to its association with the SPB, where a fraction of Sad1 and Kms1 reside. A model in which DSBs display MT-dependent mobility could explain less efficient GC using chromosome III for interallele HDR in *kms1*Δ or *mto1*Δ cells and is reminiscent of the finding that tethering of a DSB to the NE increases GC rates (Nagai *et al.*, 2008), whereas loss of Mps3 can reduce gross chromosomal rearrangements that occur in a *slx5*Δ/*slx8*Δ background (Oza *et al.*, 2009). Although we have not observed that Kms2 acts redundantly with Kms1 at non-SPB sites, it is possible that Kms2 contributes to DSB mobility at persistent, SPB-associated DSBs and/or that the copy number of Kms2 at non-SPB sites is not sufficient to be visualized. A partial redundancy of Kms1 and Kms2 could explain the more dramatic effects on DSB repair that we observe in *mto1*Δ cells (Figure 5A and Supplemental Figure S5D).

The increase in Sad1 intensity at MMS-induced foci in the absence of Kms1 or MTs suggests that resolution of NE-associated DSBs (or association of DSBs with the SPB region) is impaired under these circumstances. This may allow for accumulation of more Sad1

protomers over time or an inhibition of their dispersal. Although we cannot directly assess the fate of these DSBs, the insensitivity of the *kms1*Δ strain to DNA-damaging agents suggests that these DSBs can ultimately be repaired (Figure 6E′). Inefficient HDR (as seen in *rad51*Δ cells) may increase the likelihood that DSBs are heavily resected and recruited to the NE (Figure 6, B′ and C) and/or are slow to resolve (Figure 6, E′ and F). Both interpretations are consistent with the observation that more Sad1-Kms1 complexes form even in the absence of exogenous damage in *rad51*Δ cells (Figure 3F). Given that loss of Kms1 suppresses the growth defect seen in *rad51*Δ cells, bypassing association with the fully assembled LINC complex when HDR is impaired may better support latent repair through other, alternative pathways (Figure 6E′).

Potential roles for cytoskeletal forces in mitotic DSB repair

Oza *et al*. (2009) suggested that sequestration of DSBs at the nuclear periphery through interactions with the *S. cerevisiae* SUN protein Mps3 promoted GC. It is unclear, however, whether Mps3 is linked to the cytoskeleton through bridging proteins and, if so, whether this affects DNA repair. Using the *S. pombe* system, we provide evidence that cytoplasmic MT dynamics can contribute to HDR. Although the precise mechanisms by which mobility and/or force contribute to DSB repair remain to be defined, its role in meiosis provides potential clues, particularly as our data suggest that association of DSBs with dynamic cytoplasmic MTs promotes interallele HDR. In *C. elegans*, it has been shown that forces generated in the cytoplasm play at least two essential roles in homologue pairing during meiotic prophase I. First, the connection between chromosomes and the cytoskeleton via the LINC complex provides directed movement that increases the rate at which chromosomes may encounter one another, similar to our observation that SPB-associated DSBs are more mobile than their non–SPB- associated counterparts (Figure 3E). Second, when two chromosomes encounter one another, force is exerted on the pair to oppose synapsis of nonhomologous chromosomes (Sato *et al*., 2009) while also contributing directly to the efficiency of synapsis between homologous chromosomes (Wynne *et al*., 2012). Thus cytoskeletal forces both may act as a stringency test before synapsis and also promote synapsis by favoring a linear, in-phase arrangement of homologous chromosomes (Koszul and Kleckner, 2009; Wynne *et al*., 2012). Of interest, it is the Sad1-Kms1 LINC complex that connects telomeres to MTs and promotes fidelity of homologue pairing in meiotic prophase in *S. pombe* (Niwa *et al*., 2000; Yoshida *et al*., 2013).

The data presented here suggest that slow-to-repair DSBs that arise in G2 of the mitotic cell cycle may access a corollary of this meiotic pathway. In this context, association of DSBs with MTs through the Sad1-Kms1 LINC complex may allow DSBs to encounter a larger number of potential chromosomal loci to be used as donor sequences for repair, particularly when the sister chromatid fails as a template. In addition, the association of DSBs with the LINC complex may contribute to the evaluation of donor sequences for HDR. Such a mechanism would support latent HDR using the sister chromatid or homologous chromosome as a template. This pathway might be particularly important for DSBs that arise in repetitive DNA that is enriched at the NE, as the genome contains many potential templates with short-range homology for these regions.

MATERIALS AND METHODS

Cell culture and strain generation

The strains used in this study are listed in Supplemental Table S1. *S. pombe* cells were grown and maintained in standard cell culture conditions as described (Moreno *et al*., 1991). All strains were grown at 30°C. Gene replacements were made by exchanging the open reading frames with the kanMX6 (Bähler *et al*., 1998), hphMX6, natMX6 (Hentges *et al*., 2005), or ura4+ cassette. C-terminal GFP tagging was performed with pFa6a-GFP-kanMX6 (Bähler *et al*., 1998). The pFa6a-mCherry-kanMX6 cassette was used as a template for C-terminal mCherry tagging (Snaith *et al*., 2005). N-terminal GFP tagging was performed as established using pFa6a-kanMX6-nmt41-GFP (Bähler *et al*., 1998). N-terminal HA tagging of Kms1 under the endogenous promoter was performed by disrupting the open reading frame after the ATG start site with the ura4+ cassette. This insertion was then replaced with the HA sequence with flanking targeting sequences by selection on 5-fluoroorotic acid (resulting sequence shown in Supplemental Figure S2D). The HO site-kanMX4 was amplified from strain LLD3716 (Du *et al*., 2006) and inserted ~3 kb from *ade8* between SPBC14F5.10c and *mug186*, followed by marker switching from kanMX4 to hphMX6, in the generation of strains MKSP411, MKSP1185, and MKSP1498. The same strategy was used to insert the HO site ~8 kb upstream from *ade3* between SPAC6F12.08c and *rdp1* (strains MKSP1674 and MKSP1676). All strains generated by cassette integration were checked with PCR. Strains made through genetic crosses were confirmed by segregation of markers or presence of the appropriate fluorescently tagged protein.

Microscopy

Unless otherwise indicated, *S. pombe* strains were grown in yeast extract supplemented with uracil, leucine, lysine, histidine, and adenine (YE5S) plus 250 mg/l of adenine to log phase (OD_{600} 0.5–1.0). Cells were mounted on agarose pads (1.4% agarose in Edinburgh minimal media) and sealed with VALAP (1:1:1, vaseline:lanolin:paraffin). Live-cell images were acquired on a DeltaVision Widefield Deconvolution Microscope (Applied Precision/GE Healthcare, Issaquah, WA) with a CoolSnap HQ^2 CCD camera (Photometrics, Tucson, AZ) or an Evolve 512 electron-multiplying charge-coupled device (EM-CCD) camera (Photometrics). Imaging parameters for each experiment are indicated in the figure legends. Percentages of foci per cell are averages from images acquired in three independent experiments in which a minimum of 100 cells per time point per experiment were analyzed and are plotted as means ± SD. Relative iMTOC focus intensity was determined from images acquired using identical imaging parameters, followed by measuring the integrated density of Sad1-mCherry in iMTOCs and dividing that density by the integrated density of Sad1-mCherry at the SPB of the same cell. Intensity is displayed using a box-and-whiskers plot; the bottom and the top of the box display the first and third quartiles, respectively, and the band inside the box represents the second quartile (= median); the plus sign marks the mean. Statistical significance was determined using chi-squared tests on multinomial distributions and multiple *t* tests for relative intensity data comparisons.

Induction of HO nuclease and quantification

Strains containing the HO site integrated at *ade8* or *ade3* were transformed with the plasmid pREP41-HO, created by site-directed mutagenesis to partially repair the TATA box mutation (Basi *et al*., 1993) from pREP81-HO (Prudden *et al*., 2003), and selected on EMM –Leu with thiamine. Several colonies were inoculated into 2 ml of EMM –Leu with (to maintain repression) or without (to induce expression) thiamine for asynchronous induction. After 6–8 h of growth at 30°C, the cells were further diluted 1:10 in fresh EMM –Leu with or without thiamine and allowed to grow overnight. For G1 arrest,

the same protocol was followed, except that cells were inoculated into 2 ml of EMM –Leu –nitrogen (±thiamine) and allowed to arrest over the time course of the induction. Images/movies were taken at 24 h after initiating induction. Images were acquired every 150 s for 30 min for *ade8* and every 30 s for 10 min for *ade3*. For asynchronous cultures, mitotic cells were excluded, and individual cells were counted as "colocalized" only if the Rad52 focus remained associated with Sad1-GFP or GFP-Kms1 for the entire time course. For G1-arrested cells, single *Z*-stacks were obtained, and colocalization was determined. In all cases, plots display the mean ± SD from images acquired in three independent experiments in which a minimum of 50 cells/experiment were analyzed.

Reverse transcription PCR

Total cellular RNA was extracted using the hot phenol method. cDNA was made by reverse transcription using oligo dT primers. Primers to amplify *kms1* were designed across the first intron to allow for discrimination of templates derived from genomic DNA and the spliced transcript.

Western blotting

Protein samples were collected from yeast strains using NaOH/trichloroacetic acid protein extraction and precipitation. For MMS-treated cells, log-phase cultures were treated with 0.1% MMS for the indicated number of hours, and then total protein was extracted. The primary anti-HA.11 mouse antibody (Covance, Princeton, NJ) and anti-actin antibody (ab8824; Abcam, Cambridge, MA) were each diluted 1:1000. Chemiluminescence was used to detect the nitrocellulose membrane signal (Pierce/Thermo Scientific, Rockford, IL). Goat anti-mouse horseradish peroxidase–labeled antibody (Pierce/Thermo Scientific) was diluted 1:10,000.

Genetic interactions

For growth assays, 5-ml cultures were grown in YE5S to saturation. A 10-fold serial dilution was performed, and the dilution series was plated to YE5S or YE5S with 0.001% MMS, 0.005% MMS, 2.5 mM hydroxyurea, 5 mM hydroxyurea, or 5 μM camptothecin, as indicated. Differential epistasis was calculated by subtracting the epistasis deviation of double-knockout cells on plates containing HU from YE5S plates. The average colony size for each strain was measured from cells plated on the same day. The epistasis was calculated as a ratio of average colony size for knockout strains relative to the average colony size of WT. An epistasis value of 1 indicates that the knockout strain has the same growth as WT cells. The epistasis value of the two single-knockout strains was multiplied to give the expected epistasis value of the double-knockout strain. The expected epistasis was subtracted from the actual epistasis value of the double knockout (growth relative to WT) to determine the deviation (Collins *et al.*, 2006; Bandyopadhyay *et al.*, 2010). The differential epistasis was calculated for three biological replicates.

Repair pathway choice analysis

Inducible DSB repair pathway choice analysis was performed as described (Prudden *et al.*, 2003). The experiment was performed a minimum of three times per strain, with a minimum of 300 cells being analyzed in each condition. Statistical significance was determined using chi-squared tests of multinomial distributions.

ACKNOWLEDGMENTS

We are indebted to the Yeast Genomic Resource Center at Osaka University for access to *S. pombe* strains, as well as to the many researchers who have contributed to this resource. We also thank the laboratories of Paul Nurse, Tim Humphrey, and Paul Russell for providing additional strains. For valuable feedback during preparation of the manuscript, we thank members of the King lab, Patrick Sung, and Patrick Lusk. We thank Julien Berro and Kristen Swithers for assistance with statistical analysis. This work was supported by the G. Harold and Leila Y. Mathers Charitable Foundation, the Searle Scholars Program, the National Institutes of Health, Office of the Director, DP2OD008429-01 (to M.C.K.), and training grants T32GM007499 and 2T32GM007324-36A1 from the National Institute of General Medical Sciences (to R.K.S.).

REFERENCES

Bandyopadhyay *et al.* (2010). Rewiring of genetic networks in response to DNA damage. Science 330, 1385–1389.

Basi G, Schmid E, Maundrell K (1993). TATA box mutations in the *Schizosaccharomyces pombe* nmt1 promoter affect transcription efficiency but not the transcription start point or thiamine repressibility. Gene 123, 131–136.

Bass HW, Riera-Lizarazu O, Ananiev EV, Bordoli SJ, Rines HW, Phillips RL, Sedat JW, Agard DA, Cande WZ (2000). Evidence for the coincident initiation of homolog pairing and synapsis during the telomere-clustering (bouquet) stage of meiotic prophase. J Cell Sci 113, 1033–1042.

Beranek DT (1990). Distribution of methyl and ethyl adducts following alkylation with monofunctional alkylating agents. Mutat Res 231, 11–30.

Bähler J, Wu JQ, Longtine MS, Shah NG, McKenzie A, Steever AB, Wach A, Philippsen P, Pringle JR (1998). Heterologous modules for efficient and versatile PCR-based gene targeting in *Schizosaccharomyces pombe*. Yeast 14, 943–951.

Chikashige Y, Haraguchi T, Hiraoka Y (2007). Another way to move chromosomes. Chromosoma 116, 497–505.

Collins SR, Schuldiner M, Krogan NJ, Weissman JS (2006). A strategy for extracting and analyzing large-scale quantitative epistatic interaction data. Genome Biol 7, R63.

Ding DQ, Tomita Y, Yamamoto A, Chikashige Y, Haraguchi T, Hiraoka Y (2000). Large-scale screening of intracellular protein localization in living fission yeast cells by the use of a GFP-fusion genomic DNA library. Genes Cells 5, 169–190.

Ding DQ, Yamamoto A, Haraguchi T, Hiraoka Y (2004). Dynamics of homologous chromosome pairing during meiotic prophase in fission yeast. Dev Cell 6, 328–341.

Du L-L, Nakamura TM, Russell P (2006). Histone modification-dependent and -independent pathways for recruitment of checkpoint protein Crb2 to double-strand breaks. Genes Dev 20, 1583–1596.

Ferretti LP, Lafranchi L, Sartori AA (2013). Controlling DNA-end resection: a new task for CDKs. Front Genet 4, 99.

Gartenberg MR (2009). Life on the edge: telomeres and persistent DNA breaks converge at the nuclear periphery. Genes Dev 23, 1027–1031.

Hagan I, Yanagida M (1995). The product of the spindle formation gene sad1+ associates with the fission yeast spindle pole body and is essential for viability. J Cell Biol 129, 1033–1047.

Hentges P, Van Driessche B, Tafforeau L, Vandenhaute J, Carr AM (2005). Three novel antibiotic marker cassettes for gene disruption and marker switching in *Schizosaccharomyces pombe*. Yeast 22, 1013–1019.

Horio T, Uzawa S, Jung MK, Oakley BR, Tanaka K, Yanagida M (1991). The fission yeast gamma-tubulin is essential for mitosis and is localized at microtubule organizing centers. J Cell Sci 99, 693–700.

Kalocsay M, Hiller NJ, Jentsch S (2009). Chromosome-wide Rad51 spreading and SUMO-H2A.Z-dependent chromosome fixation in response to a persistent DNA double-strand break. Mol Cell 33, 335–343.

Kim D-U *et al.* (2010). Analysis of a genome-wide set of gene deletions in the fission yeast *Schizosaccharomyces pombe*. Nat Biotechnol 28, 617–623.

King MC, Drivas TG, Blobel G (2008). A network of nuclear envelope membrane proteins linking centromeres to microtubules. Cell 134, 427–438.

Koszul R, Kleckner N (2009). Dynamic chromosome movements during meiosis: a way to eliminate unwanted connections?. Trends Cell Biol 19, 716–724.

Labib K, De Piccoli G (2011). Surviving chromosome replication: the many roles of the S-phase checkpoint pathway. Philos Trans R Soc Lond B Biol Sci 366, 3554–3561.

Langerak P, Mejia-Ramirez E, Limbo O, Russell P (2011). Release of Ku and MRN from DNA ends by Mre11 nuclease activity and Ctp1 is required

for homologous recombination repair of double-strand breaks. PLoS Genet 7, e1002271.
Lei K, Zhu X, Xu R, Shao C, Xu T, Zhuang Y, Han M (2012). Inner nuclear envelope proteins SUN1 and SUN2 play a prominent role in the DNA damage response. Curr Biol 22, 1609–1615.
Malkova A, Haber JE (2012). Mutations arising during repair of chromosome breaks. Annu Rev Genet 46, 455–473.
Marguerat S, Schmidt A, Codlin S, Chen W, Aebersold R, Bähler J (2012). Quantitative analysis of fission yeast transcriptomes and proteomes in proliferating and quiescent cells. Cell 151, 671–683.
McGee MD, Stagljar I, Starr DA (2009). KDP-1 is a nuclear envelope KASH protein required for cell-cycle progression. J Cell Sci 122, 2895–2905.
Moreno S, Klar A, Nurse P (1991). Molecular genetic analysis of fission yeast *Schizosaccharomyces pombe*. Meth Enzymol 194, 795–823.
Muris DF, Vreeken K, Schmidt H, Ostermann K, Clever B, Lohman PH, Pastink A (1997). Homologous recombination in the fission yeast *Schizosaccharomyces pombe*: different requirements for the rhp51+, rhp54+ and rad22+ genes. Curr Genet 31, 248–254.
Nagai S, Dubrana K, Tsai-Pflugfelder M, Davidson MB, Roberts TM, Brown GW, Varela E, Hediger F, Gasser SM, Krogan NJ (2008). Functional targeting of DNA damage to a nuclear pore-associated SUMO-dependent ubiquitin ligase. Science 322, 597–602.
Niwa O, Shimanuki M, Miki F (2000). Telomere-led bouquet formation facilitates homologous chromosome pairing and restricts ectopic interaction in fission yeast meiosis. EMBO J 19, 3831–3840.
Osman F, Fortunato EA, Subramani S (1996). Double-strand break-induced mitotic intrachromosomal recombination in the fission yeast *Schizosaccharomyces pombe*. Genetics 142, 341–357.
Oza P, Jaspersen SL, Miele A, Dekker J, Peterson CL (2009). Mechanisms that regulate localization of a DNA double-strand break to the nuclear periphery. Genes Dev 23, 912–927.
Prudden J, Evans JS, Hussey SP, Deans B, O'Neill P, Thacker J, Humphrey T (2003). Pathway utilization in response to a site-specific DNA double-strand break in fission yeast. EMBO J 22, 1419–1430.
Razafsky D, Hodzic D (2009). Bringing KASH under the SUN: the many faces of nucleo-cytoskeletal connections. J Cell Biol 186, 461–472.
Rudin N, Haber JE (1988). Efficient repair of HO-induced chromosomal breaks in *Saccharomyces cerevisiae* by recombination between flanking homologous sequences. Mol Cell Biol 8, 3918–3928.
Sato A, Isaac B, Phillips CM, Rillo R, Carlton PM, Wynne DJ, Kasad RA, Dernburg AF (2009). Cytoskeletal forces span the nuclear envelope to coordinate meiotic chromosome pairing and synapsis. Cell 139, 907–919.
Sauvageau S, Stasiak AZ, Banville I, Ploquin M, Stasiak A, Masson J-Y (2005). Fission yeast rad51 and dmc1, two efficient DNA recombinases forming helical nucleoprotein filaments. Mol Cell Biol 25, 4377–4387.
Sawin KE, Lourenco PCC, Snaith HA (2004). Microtubule nucleation at non-spindle pole body microtubule-organizing centers requires fission yeast centrosomin-related protein mod20p. Curr Biol 14, 763–775.
Sawin KE, Tran PT (2006). Cytoplasmic microtubule organization in fission yeast. Yeast 23, 1001–1014.
Scherthan H, Weich S, Schwegler H, Heyting C, Härle M, Cremer T (1996). Centromere and telomere movements during early meiotic prophase of mouse and man are associated with the onset of chromosome pairing. J Cell Biol 134, 1109–1125.
Shimanuki M, Miki F, Ding DQ, Chikashige Y, Hiraoka Y, Horio T, Niwa O (1997). A novel fission yeast gene, kms1+, is required for the formation of meiotic prophase-specific nuclear architecture. Mol Gen Genet 254, 238–249.
Shiotani B, Zou L (2009). Single-stranded DNA orchestrates an ATM-to-ATR switch at DNA breaks. Mol Cell 33, 547–558.
Snaith HA, Samejima I, Sawin KE (2005). Multistep and multimode cortical anchoring of tea1p at cell tips in fission yeast. EMBO J 24, 3690–3699.
Sosa BA, Rothballer A, Kutay U, Schwartz TU (2012). LINC complexes form by binding of three KASH peptides to domain interfaces of trimeric SUN proteins. Cell 149, 1035–1047.
Straight AF, Belmont AS, Robinett CC, Murray AW (1996). GFP tagging of budding yeast chromosomes reveals that protein-protein interactions can mediate sister chromatid cohesion. Curr Biol 6, 1599–1608.
Symington LS, Gautier J (2011). Double-strand break end resection and repair pathway choice. Annu Rev Genet 45, 247–271.
Tapley EC, Starr DA (2012). Connecting the nucleus to the cytoskeleton by SUN-KASH bridges across the nuclear envelope. Curr Opin Cell Biol 25, 57–62.
Tomimatsu N, Mukherjee B, Hardebeck MC, Ilcheva M, Camacho CV, Harris JL, Porteus M, Llorente B, Khanna KK, Burma S (2014). Phosphorylation of EXO1 by CDKs 1 and 2 regulates DNA end resection and repair pathway choice. Nat Commun 5, 3561.
Vazquez J, Belmont AS, Sedat JW (2002). The dynamics of homologous chromosome pairing during male *Drosophila* meiosis. Curr Biol 12, 1473–1483.
Venkatram S, Tasto JJ, Feoktistova A, Jennings JL, Link AJ, Gould KL (2004). Identification and characterization of two novel proteins affecting fission yeast gamma-tubulin complex function. Mol Biol Cell 15, 2287–2301.
Wälde S, King MC (2014). The KASH protein Kms2 coordinates mitotic remodeling of the spindle pole body. J Cell Sci, jcs.154997.
Wu J-Q, Pollard TD (2005). Counting cytokinesis proteins globally and locally in fission yeast. Science 310, 310–314.
Wynne DJ, Rog O, Carlton PM, Dernburg AF (2012). Dynein-dependent processive chromosome motions promote homologous pairing in *C. elegans* meiosis. J Cell Biol 196, 47–64.
Yoshida M *et al.* (2013). Microtubule-organizing center formation at telomeres induces meiotic telomere clustering. J Cell Biol 200, 385–395.